Collapse at the eastern Eiger flank in the Swiss Alps

THIERRY OPPIKOFER[1]*, MICHEL JABOYEDOFF[1] AND HANS-RUDOLF KEUSEN[2]

[1]Institute of Geomatics and Analysis of Risk (IGAR), University of Lausanne, 1015 Lausanne, Switzerland

[2]Geotest AG, 3052 Zollikofen, Switzerland

*e-mail: thierry.oppikofer@unil.ch

Published online: 27 July 2008; doi:10.1038/ngeo258

Landslides are a significant natural hazard in mountainous regions[1] and are often triggered by external factors, such as earthquakes, rainfall, permafrost melting or retreat of glaciers[2]. A large landslide occurred in the Swiss Alps on 13 July 2006, when portions of an immense rock spur on the eastern flank of the Eiger peak[3] collapsed. Here we use field observations and terrestrial laser scanning data to record and quantify the relative motion along the various blocks of rock that form this spur. The data show that during the year of observation the blocks moved relative to one another by up to tens of metres along fractures that can be related to pre-existing planes of weakness. Rates of motion and deformation were high throughout July 2006, particularly in the northern part of the spur that partially collapsed on 13 July. The rates decreased considerably during the subsequent months, although a slight increase was noted in June and July 2007. These observations are consistent with instability of the spur initiated by subsidence of a single block at the rear, which acted as a wedge and disintegrated over time owing to loss of lateral confinement.

Recent catastrophic events in the Swiss Alps illustrate the necessity of efficient monitoring of landslides: heavy rainfall caused a landslide resulting in 14 deaths in October 2000 (ref. 4); intense precipitation triggered debris flows, mud flows and rockfalls killing five people in August 2005 (refs 5,6) and a major rockfall killed two persons on a national highway in May 2006 (ref. 7).

High-resolution digital elevation models obtained from aerial or terrestrial laser scanning are used to detect landslides and rockfalls[8–17]. Most landslide monitoring techniques provide information on only a few selected points and not the whole landslide surface[11]. Sequential terrestrial laser scanning (TLS), on the other hand, allows for analysis of movement direction and velocity, displacement and volume change[9–13]. These three-dimensional data open new perspectives in predicting mass wasting and deciphering failure mechanisms.

In this study, we focus on a collapse at the Eiger's eastern flank (Fig. 1a), one of Switzerland's most famous peaks. The instability of this 2 million m^3, compact Jurassic limestone mass was caused by the Lower Grindelwald glacier's retreat, which has been accelerated since 1935 by global warming[18,19]. At the last glacier maximum in 1860, the ice reached the back scar's level[19,20]. The instability was subject to particularly high glacial compression due to its position on a topographic ridge[21]. The removal of the glacier buttress and subsequent decompression allowed the spur to fail.

On 10 June 2006 rockfalls of several hundred m^3, first slope movements and two steep 250-m-long valley-parallel open cracks were observed. One of these fractures forms the back-crack of the spur, and the other separates the spur into a front and a rear block (Fig. 1b,c). In addition, these blocks are separated into a main part and a northern part by a subvertical bedding plane that is nearly perpendicular to the open cracks (Fig. 1b). On 11 July 2006, we deployed a long-range terrestrial laser scanner to monitor the rockslide (see the Methods section) and acquired sequential TLS point clouds on 12, 13, 17 and 25 July, 22 September and 1 December 2006, and on 11 June and 17 July 2007 (photographs in Supplementary Information, Fig. S1). The comparison of sequential point clouds reveals the instability's displacements (Fig. 2, Supplementary Information, Fig. S2) and enables the calculation of rockfall volumes. During the first days of TLS monitoring, the rear block subsided with a velocity of up to 80 cm d^{-1}, whereas the front block slid forward with a velocity of about 20 cm d^{-1}, which is unusually high for hard rock slopes (Fig. 2a).

On the northern front block, frequent rockfalls were recorded (rockfall volume: 2,530 m^3 between 11 and 12 July 2006, and 450 m^3 in the following 24 h). A column showed significantly higher movement rates, up to 125 cm d^{-1} (Fig. 2a), which led to its collapse and finally to a partial collapse of the northern block on 13 July 2006 (Fig. 1d) with a computed volume of 169,000 m^3. Slope movements continued, but with lower velocities (60 cm d^{-1} and 15 cm d^{-1} for the rear and front blocks, respectively, between 13 and 17 July 2006) (Fig. 2b). We did not detect new large rockfalls on sequential TLS datasets in the following months. Nonetheless, the rock mass continued to move, but with lower velocities (4 cm d^{-1} and 1.5 cm d^{-1} for the rear and front blocks, respectively, during winter 2006/2007; see Supplementary Information, Fig. S2). Our surveys in summer 2007 showed an increase in the rear block's movement (up to 15 cm d^{-1}). The front block's displacement rates reveal some toppling with higher velocities at its top ($\sim$9 cm d^{-1}) relative to its toe ($\sim$6 cm d^{-1}).

For a more precise slope movement analysis, we computed displacement vectors. Their orientation remained similar between July and September 2006, but their magnitude decreased (Fig. 3, Supplementary Information, Fig. S3 and Table S1). The front block moved towards 041°/35° (plunge direction/plunge), whereas the rear block was mainly subsiding (007°/68° between July and September 2006). Since autumn 2006, the rear block's movement direction has turned more to the east owing to disintegration and toppling towards the east (Supplementary Information, Fig. S3 and Supplementary Information, Table).

The structural analysis on the basis of the TLS point clouds (see the Methods section) reveals three main discontinuity sets

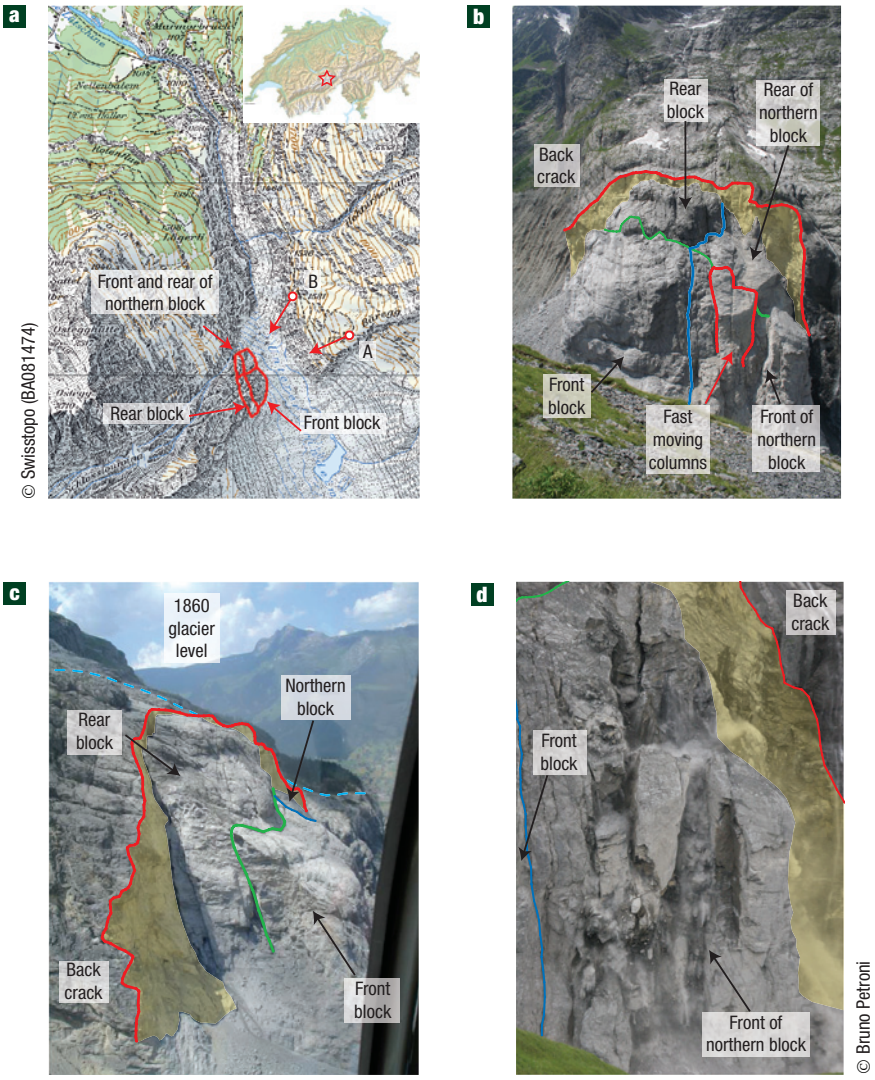

Figure 1 Geographical setting of the 2006 Eiger rockslide. a, Location map indicating the different blocks of the Eiger rockslide, and the scanning locations (A and B) and directions. **b**, Frontal view of the Eiger rockslide (12 July 2006). The spur is divided into a front and a rear block separated by a steep middle fracture (green line). Northern rear and front blocks are separated from the main blocks by a bedding plane (blue line). **c**, Lateral view of the instability (4 July 2006). **d**, Photograph of the northern blocks' partial collapse on 13 July 2006.

(Fig. 3a): slightly undulating bedding planes S_0 with orientations varying between 135°/80° (dip direction/dip angle) and 313°/71°; discontinuity set J_1 dipping towards the valley (067°/36° ± 2.9°) and set J_2 parallel to the valley (060°/78° ± 2.9°). The back-crack and the middle fracture, separating the front block from the rear, are formed by sets J_2 and S_0 and their overall orientations are 076°/81° and 072°/89°, respectively. The discontinuity sets are of tectonic origin, but their opening is related to debuttressing.

On the basis of the structural data we established an instability mechanism that explains the observed three-dimensional slope displacements (Figs 3,4). The front block slides on a basal failure surface formed by discontinuity set J_1 (067°/36°), which was laterally constrained by the bedding planes S_0 (mean orientation: 313°/86° ± 3.1°). In fact, the intersection $S_0 \wedge J_1$ (040°/33°) has an orientation similar to the displacement vectors of the front block (041°/35°), its toe (045°/39°) and also the northern block's front (038°/39°). The subsidence of the rear block (overall displacement vector: 026°/76°) and the northern block's rear part (031°/74°) is controlled by set J_2 and the bedding S_0 (intersection: 027°/76°).

Initially, the instability evolved as bilinear wedge failure[22], with the rear block, including the northern rear block, acting as an active wedge pushing the front and northern front block passively along the basal failure surface, in a manner comparable to the Prandtl wedge mechanism proposed for the 1963 Vaiont landslide in Italy[23,24]. The Prandtl wedge is situated along the middle fracture and consists of a zone of extensive internal rock mass deformation, because it transmits the driving forces of the rear blocks to the front blocks. The movement initiation was most likely promoted by high water pressures at the sliding plane due to snow melting and high precipitation in spring and summer 2006, which is a common triggering factor[2,25]. The rear blocks rapidly started to break apart owing to high displacements and lack of lateral confinement. Photographs (see Supplementary Information, Fig. S1) indicate that both rear blocks became more and more

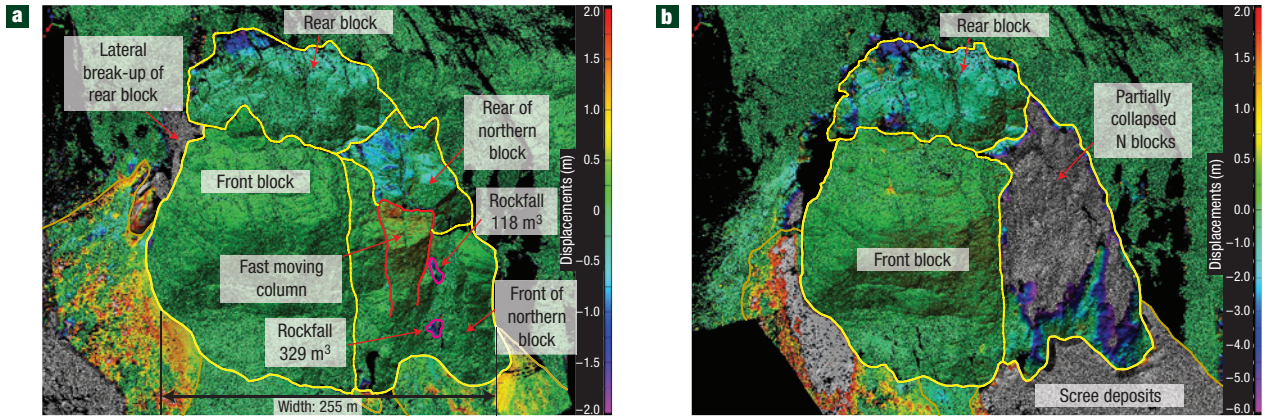

Figure 2 Comparison of sequential TLS point clouds. Green colour indicates no displacement, yellow to red colours stand for advance of the rockslide or for scree accumulation, whereas blue to violet colours express downward movements or rockfall areas. Missing data are due to wet surfaces and occlusion. **a**, Between 12 and 13 July 2006 (24 h interval) displacements up to 2 m are shown. **b**, Movements between −6 m and +2 m are shown for the 96 h period between 13 and 17 July 2006. The partially collapsed northern block appears in grey, because the differences exceed the colour scale.

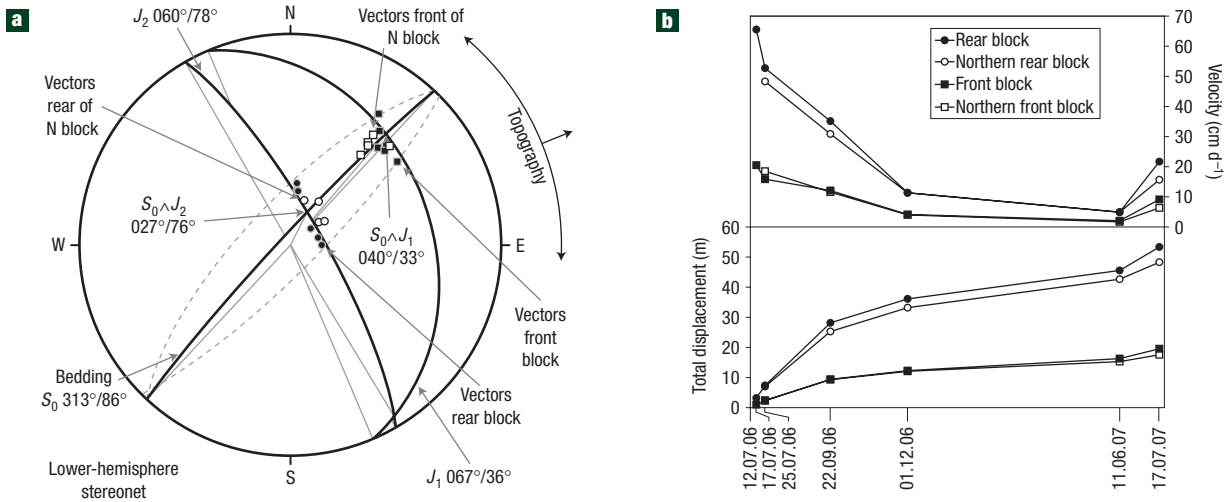

Figure 3 Spatial orientations of main discontinuity sets and displacement vectors. a, The orientation of the bedding planes varies slightly between 135°/80° and 313°/71° (stippled great circles), the mean orientation being 313°/86° (lower-hemisphere stereonet). The displacement vectors of the rear and northern rear blocks (filled and open circles, respectively) lie within the S_0/J_2 intersection, whereas the displacement vectors of the front and northern front blocks (filled and open squares, respectively) are controlled by the S_0/J_1 intersection. **b**, Graph of the total displacement since the beginning of the TLS monitoring (bottom) and the velocity (top) versus date of the TLS acquisition.

dismantled into smaller blocks, which behave more like a granular aggregate than an intact rock mass, which is in agreement with the Prandtl wedge mechanism[23]. The disintegration of the rear blocks led to a mass loss and perhaps an increase in water permeability and consequently to lower pore-water pressure along the basal failure surface. The combination of mass loss and lower pore-water pressure could explain the observed decrease in velocity at the end of summer 2006 and during winter 2006/2007. The velocity increase in summer 2007 is probably caused by rheological changes along the failure surface due to rock crushing[26] and by increased pore-water pressure due to snow melting[25]. Finally, the toppling detected in addition to the sliding of the front block suggests that its toe started to be retained by the glacier (Fig. 4).

The ability to predict failure is crucial to hazard assessment and monitoring of landslides[27]. Comparison of sequential TLS data enables the detection of areas with the highest displacement rates, which are more susceptible to future failure. The partial collapse of 13 July 2006 (Figs 1b, 2a) underlines the link between maximum velocities and failure locations. Knowing the most active zones on a landslide, permanent survey techniques can be designed for precise temporal failure prediction.

Our study demonstrates the necessity of a global analysis of three-dimensional displacements on the entire unstable body, as obtained by comparison of TLS point clouds. This enabled us to understand the failure mechanism and construct a consistent structural and geometrical instability model, with the subsiding

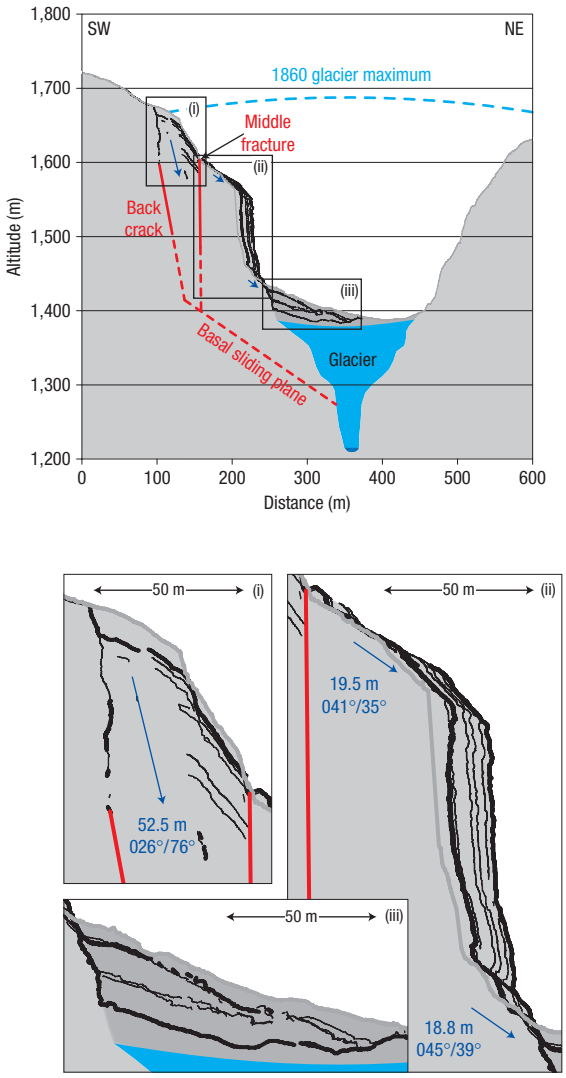

Figure 4 Profile across the Eiger rockslide. The profile is parallel to the displacement direction of the front block (southwest–northeast). The back-crack and middle fracture, as well as black cross-sections, are based on TLS data. First and last TLS data are shown as thicker black lines. The grey line illustrates the prefailure state (DEM-CS provided by swisstopo). The position of the basal sliding plane is unknown, but its orientation is controlled by J_1. Total displacement vectors between 11 July 2006 and 17 July 2007 are shown to scale. Enlargements show (i) the rear block, (ii) the front block and (iii) the scree deposits.

rear block acting as an active wedge. Such knowledge is crucial for landslide hazard assessment, because it opens new perspectives in characterizing and understanding the slope movements and helps in designing continuous monitoring techniques.

METHODS

TLS is based on the reflectorless and contactless acquisition of a point cloud of the topography using the pulsed laser time-of-flight technique[8]. For this study, we used an Optech Ilris 3D terrestrial laser scanner system and acquired TLS point clouds with 3–5 million points from two viewpoints located on the opposite side of the valley (Sites A and B in Fig. 1a) at a distance of 600 m and 530 m and with a mean angular point spacing of 0.018° and 0.021°, respectively. From both viewpoints the resulting point cloud has an average resolution of 18.0 cm on the rock face and 20.0 cm at the back-crack. This spacing is approximately twice the magnitude of the laser spot size (11.4 cm at a distance of 600 m), which is significantly more than the proposed ideal spacing of 0.859 times the beamwidth[28]. This however has the advantage of drastically reducing acquisition time and data file size by still providing high-resolution point clouds.

We aligned the scans from both viewpoints with Innovmetric PolyWorks software using first manual point-pair matching and afterwards the surface-to-surface iterative closest point algorithm implemented in PolyWorks[29]. We progressively reduced the maximum distance between the two scans to minimize the alignment errors ($1\sigma_a < 2.5$ cm). This error is mainly due to the spot spacing and the fact that consequently not always the same points of the quite irregular rock surfaces were measured. In comparison, the instrument's precision is given by the manufacturer as 7 mm on the range and 8 mm on the position at a distance of 100 m. Georeferencing is achieved by alignment of the TLS point cloud onto the high-resolution aerial digital elevation model with a cell size of 2 m (DEM-CS provided by swisstopo), with an absolute positioning error of 14.5 cm ($1\sigma_{gr}$). We used the same alignment procedure for the alignment of sequential TLS point clouds, but restraining the iterative alignment to the stable part around the rockslide only ($1\sigma_a < 2.5$ cm). Thus, the overall alignment error of sequential scans is equal to approximately 6 cm on single points. The displacements measured in the 2006 Eiger rockslide are much bigger than instrumental and data treatment errors. Considering entire point clouds, for example by interpolated surfaces, errors are significantly lower than on single points[30].

Pre- and postfailure three-dimensional models on the basis of the interpolated TLS point clouds permitted us to obtain precisely the volume of rockfalls by calculating the volume contained between the two surfaces using PolyWorks. The comparison of the aligned sequential TLS point clouds reveals differences (expressed as shortest distance) between the two topographic surfaces. These positive or negative differences are interpreted as slope movements: positive differences stand for an advance of the rockslide and debris accumulation on the scree slopes, whereas negative differences are related to subsidence or rockfalls.

More precise information on the slope movements is obtained from displacement vectors of different rockslide parts. They are calculated by manually identifying corresponding points on view-shaded representations of both point clouds. Ideal point pairs are summits of blocks or small spurs, intersections or end points of discontinuity traces and so on. The vector between a point pair provides the displacement direction and velocity of the point. Multiple vectors on each rockslide compartment provide the mean displacement vector and error. The errors in the average displacement length and orientation are obtained by dividing the standard deviations by the square root of the number of vectors and are equal to 10.1 cm and 2.7° (aperture of cone centred on the mean orientation and including 68% of the values), respectively. The relatively high error is due to the high point spacing (~18 cm), the measurement error on a single point and the fact that the slope is breaking apart.

The orientations of main discontinuity sets are obtained from the TLS data by selecting the points that define a discontinuity and fitting a plane through the point selection. As for the displacement vectors, the standard deviation of the discontinuity orientation is expressed as the cone aperture divided by the square root of the number of vectors.

Received 21 December 2007; accepted 26 June 2008; published 27 July 2008.

References

1. Evans, S. G. & Clague, J. J. Recent climatic change and catastrophic geomorphic processes in mountain environments. *Geomorphology* **10**, 107–128 (1994).
2. Wieczorek, G. F. in *Landslides Investigation and Mitigation* (eds Turner, A. K. & Schuster, R. L.) 76–90 (Transportation Research Board, National Research Council, National Academy Press, Washington DC, 1996).
3. Hopkin, M. Eiger loses face in massive rockfall. *News@Nature* <http://www.nature.com/news/2006/060717/full/060717-3.html> (2006).
4. Petrascheck, A. & Hegg, C. (eds) *Hochwasser 2000 - Les crues 2000* (Federal Office for Water and Geology, Berne, Switzerland, 2002).
5. Beniston, M. August 2005 intense rainfall event in Switzerland: Not necessarily an analog for strong convective events in a greenhouse climate. *Geophys. Res. Lett.* **33**, L05701 (2006).
6. Munich, Re. *Topics Geo - Annual Review: Natural Catastrophes 2005* (Munich Reinsurance Company, Munich, Germany, 2006).
7. Liniger, M. Die Herausforderung der Gefahrenprognose bei Massenbewegungen: Rutsch- und Sturzprozesse Markus Liniger. *Bull. Appl. Geol.* **11**, 75–88 (2006).
8. Slob, S. & Hack, R. in *Engineering Geology for Infrastructure Planning in Europe. A European Perspective* (eds Hack, R., Azzam, R. & Charlier, R.) 179–190 (Springer, Berlin, 2004).
9. Rosser, N. J., Petley, D. N., Lim, M., Dunning, S. A. & Allison, R. J. Terrestrial laser scanning for monitoring the process of hard rock coastal cliff erosion. *Q. J. Eng. Geol.* **38**, 363–375 (2005).
10. Abellán, A., Vilaplana, J. M. & Martínez, J. Application of a long-range terrestrial laser scanner to a detailed rockfall study at Vall de Núria (Eastern Pyrenees, Spain). *Eng. Geol.* **88**, 136–148 (2006).

11. Bitelli, G., Dubbini, M. & Zanutta, A. *Proc. XXth ISPRS Congress, Istanbul* Vol. 35, 246–251 (International Society for Photogrammetry and Remote Sensing, Istanbul, Turkey, 2004).
12. Rosser, N. J., Petley, D. N., Dunning, S. A., Lim, M. & Ball, S. Rock mechanics: Meeting society's challenges and demands. in *Proc. 1st Canada–U.S. Rock Mechanics Symposium, Vancouver, Canada, May 27–31, 2007* (eds Eberhardt, E., Stead, D. & Morrison, E.) 113–120 (Taylor and Francis, London, 2007).
13. Bauer, A., Paar, G. & Kaltenböck, A. in *Geo-information for Disaster Management* (eds van Oosterom, P., Zlatanova, S. & Fendel, E. M.) 393–406 (Springer, Berlin, 2005).
14. Derron, M.-H., Jaboyedoff, M. & Blikra, L. H. Preliminary assessment of rockslide and rockfall hazards using a DEM (Oppstadhornet, Norway). *Nat. Haz. Earth Syst. Sci.* **5**, 285–292 (2005).
15. Schulz, W. H. Landslide susceptibility revealed by LiDAR imagery and historical records, Seattle, Washington. *Eng. Geol.* **89**, 67–87 (2007).
16. Agliardi, F. & Crosta, G. B. High resolution three-dimensional numerical modelling of rockfalls. *Int. J. Rock Mech. Min.* **40**, 455–471 (2003).
17. McKean, J. & Roering, J. Objective landslide detection and surface morphology mapping using high-resolution airborne laser altimetry. *Geomorphology* **57**, 331–351 (2004).
18. GK/SCNAT & VAW/ETHZ. *The Swiss Glaciers, Yearbooks of the Glaciological Commission of the Swiss Academy of Science (SAS).* (http://glaciology.ethz.ch/swiss-glaciers) (Labratory of Hydraulics, Hydrology and Glaciology (VAW) of ETH Zürich, 2006).
19. Messerli, B., Messerli, P., Pfister, C. & Zumbuhl, H. J. Fluctuations of climate and glaciers in the Bernese Oberland, Switzerland, and their geoecological significance, 1600 to 1975. *Arct., Alp. Res.* **10**, 246–260 (1978).
20. OcCC. *Climate Change and Switzerland in 2050. Impacts on Environment, Society and Economy* (OcCC/ProClim-, Bern, Switzerland, 2007).
21. Sartori, M., Baillifard, F., Jaboyedoff, M. & Rouiller, J. D. Kinematics of the 1991 Randa rockslides (Valais, Switzerland). *Nat. Haz. Earth Syst. Sci.* **3**, 423–433 (2003).
22. Norrish, N. I. & Wyllie, D. C. in *Landslides Investigation and Mitigation* (eds Turner, A. K. & Schuster, R. L.) 391–425 (Transportation Research Board, National Research Council, National Academy Press, Washington DC, 1996).
23. Eberhardt, E., Stead, D. & Coggan, J. S. Numerical analysis of initiation and progressive failure in natural rock slopes—the 1991 Randa rockslide. *Int. J. Rock Mech. Min.* **41**, 69–87 (2004).
24. Mencl, V. Mechanics of landslides with non-circular slip surfaces with special reference to the Vaiont slide. *Geotechnique* **16**, 329–337 (1966).
25. Coe, J. A. *et al.* Seasonal movement of the Slumgullion landslide determined from Global Positioning System surveys and field instrumentation, July 1998–March 2002. *Eng. Geol.* **68**, 67–101 (2003).
26. Jaboyedoff, M., Baillifard, F., Bardou, E. & Girod, F. The effect of weathering on Alpine rock instability. *Q. J. Eng. Geol.* **37**, 95–103 (2004).
27. Crosta, G. B. & Agliardi, F. Failure forecast for large rock slides by surface displacement measurements. *Can. Geotech. J.* **40**, 176–191 (2003).
28. Lichti, D. D. & Jamtsho, S. Angular resolution of terrestrial laser scanners. *The Photogrammetric Record* **21**, 141–160 (2006).
29. Guarnieri, A., Pirotti, F., Pontin, M. & Vettore, A. *3rd IAG/12th FIG Symp., Baden, Austria* (International Association of Geodesy & International Federation of Surveyors, Baden, Austria, 2006).
30. Lindenbergh, R. & Pfeifer, N. *Proc. 7th Conf. Optical 3D Measurement Techniques, Vienna, Austria* Vol. 2, 61–70 (Vienna University of Technology, Vienna, Austria, 2005).

Supplementary Information accompanies this paper on www.nature.com/naturegeoscience.

Acknowledgements

We thank A. Pedrazzini, M. Frayssines, M. Dessimoz, J. Travelletti and R. Minoia from the University of Lausanne, P. Städelin and D. Weder from Geotest AG, C. Reymond and C. Rochat for assistance in the field and G. B. Crosta from the University of Milano—Bicocca and D. Stead from the Simon Fraser University for suggestions and comments on the manuscript.

Author contributions

T.O. acquired and analysed the terrestrial laser scanner data. T.O. and M.J. elaborated the model of the instability and drafted the paper. All the authors contributed to discussing the results and finalizing the manuscript.

Author information

Reprints and permission information is available online at http://npg.nature.com/reprintsandpermissions. Correspondence and requests for materials should be addressed to T.O.